ELSEVIER

Journal of Contaminant Hydrology 41 (2000) 317–334

JOURNAL OF Contaminant Hydrology

www.elsevier.com/locate/jconhyd

Surfactant-induced changes in gravity fingering of water through a light oil

David A. DiCarlo [a], Tim W.J. Bauters [b], Christophe J.G. Darnault [b], Eva Wong [b], Barnes R. Bierck [b], Tammo S. Steenhuis [b,*], J.-Yves Parlange [b]

[a] *Department of Petroleum Engineering, Stanford University, Stanford, CA 94305, USA*
[b] *Department of Agricultural and Biological Engineering, Cornell University, Ithaca, NY 14853, USA*

Received 28 April 1998; accepted 23 August 1999

Abstract

Gravity-driven preferential flow (fingering) can greatly affect how one fluid displaces another in the subsurface. We have studied the internal properties of these preferential flow paths for water, with and without surfactants, infiltrating into oil saturated porous media using synchrotron X-rays, and miniature tensiometers to characterize fluid content and pressure relationships. We also used a light transmission technique to visualize overall flow pattern. Capillary pressure and water content decrease behind the front, similar to fingers in air-dry sand, with quantitative differences for five different surfactants with surface tensions ranging from 4–21 g/s^2. Using unstable flow theory, the finger widths, capillary pressure drops within the fingers, finger tip lengths, and finger splitting dynamics were scaled successfully with interfacial tension, fluid density, and the contact angle using the fingers in air–water systems as the reference.

Keywords: Preferential flow; Tomograpy; Two-phase flow; Constitutive relationship; Interfacial tension; X-rays

1. Introduction

Preferential flow, which can occur when one fluid displaces another fluid in a porous media, will greatly affect the transport and emplacements of fluids in processes

* Corresponding author. Tel.: +1-607-255-2489; fax: +1-607-255-4080; e-mail: tss1@cornell.edu

0169-7722/00/$ - see front matter
PII: S0169-7722(99)00078-9

including water infiltration, enhanced oil recovery, and remediation efforts. In uniform media, preferential flow is a result of the fluid interface being unstable during a displacement. Saffman and Taylor (1958) presented a criterium for instability when fluid 1 displaces fluid 2,

$$kg(\rho_1 - \rho_2) - u(\theta_f - \theta_i)(\mu_1 - \mu_2) > 0 \quad (1)$$

where k is the permeability of the media, g is the gravitational acceleration, ρ is the fluid density, u is the unperturbed front velocity, θ_f and θ_i are the final and initial invading fluid contents, and μ is the viscosity. Eq. (1) does not include the wetting properties of the porous medium and the interfacial tension between the fluids which affect the widths of the resultant fingers (Parlange and Hill, 1976). Much of the work on instabilities when an aqueous phase displaces a non-aqueous phase has been in the viscous fingering limit, where the density force is negligible (Homsy, 1987). By assuming an abrupt interface between the phases, Chuoke et al. (1959) accounted for the capillary effects of the porous medium by an ''effective'' surface tension.

Concurrently, soil scientists have been interested in preferential flow during infiltration events, when the flow rate is slow and the fingering is driven by density effects (Hill and Parlange, 1972). In the case of water infiltrating air-dry soil, Parlange and Hill (1976) accounted for the capillary effects of the porous media by treating the wetting front as diffuse. The resultant expression for the finger dimensions includes the sorptivity, S, of the soil which is a function of the unsaturated hydraulic conductivity and the capillary pressure–fluid content relationships. Recently, this has been extended to water infiltrating into oil-saturated soils by Chandler et al. (1998) with the assumption that the flux is low enough to eliminate viscous effects in the oil.

Most experimental studies have focused on fingering in Hele–Shaw cells or at the outside wall of thin sands due to the difficulty in ''seeing'' inside a complete porous media. Viscous fingering has been studied as a function of front velocity, interfacial tension, and wettability in Hele–Shaw cells (Homsy, 1987) and at the wall of thin glass bead packs (Stokes et al., 1986). Of particular interest is the use of surfactants or detergents in the aqueous phase, which are used for enhanced oil recovery or remediation. By altering the interfacial properties with a surfactant, the preferential flow properties change dramatically (Bensimon et al., 1986; Homsy, 1987).

Inside porous media, the fluid content at and behind the interface can show wide variations and affect the scale of the preferential flow (Glass et al., 1988; Selker et al., 1992b; Liu et al., 1994b; Bauters et al., 1999). In this paper, we have used synchrotron X-ray attenuation to measure fluid contents accurately and quickly during fingering within a two-dimensional slab of a three-dimensional porous media. Along with fast measurements of the fluids' pressures, a better understanding of the dynamics of fingering can be resolved. By using sands already well characterized for fingers through dry sand, we find that the fingers through oil are qualitatively similar and the quantitative differences can be directly related to the interfacial tension and the density differences of the fluids. Thus, the same physics of unstable fluid displacements can be used to describe and predict gravity-driven fingered flow for many fluid pairs.

2. Theory

We wish to obtain expressions for finger width and the fluid energy state (pressure) inside the finger for the case of water with a surfactant infiltrating an oil saturated column. The capillary pressure, h_c, (given in units of head), which is the pressure difference between the non-wetting (h_{nw}) and wetting (h_w) phase, is related to the pore radius (r) through the Laplace equation (Lenhard and Parker, 1987),

$$h_c = h_{nw} - h_w = \frac{2\sigma_{w/nw}\cos(\varphi_{w/nw})}{\rho_w g r} \tag{2}$$

where ρ_w is the bulk density of water, g is the gravity constant, the subscript w/nw refers to each particular wetting and non-wetting fluid pair, σ is the interfacial tension of the pair, and φ is the contact angle. Thus, in a fixed porous medium, the capillary pressure–fluid content (h_c–θ) relationship for a fluid pair will scale with the products of interfacial tension and cosine of the contact angle between the fluid pairs. In particular, the two-phase water–oil (h_c–θ) relationship can be related to the two-phase water–air relationship through,

$$h_{w/o}(\theta_w) = R\frac{\sigma_{w/o}}{\sigma_{w/a}} h_{w/a}(\theta_w) \tag{3}$$

where R is the ratio of cosines of the contact angles for water–oil and water–air fluid pairs. The oil is the non-wetting phase and we will use the subscript o. Also, the relationship is always hysteretic, depending on if the wetting fluid is entering (wetting) or leaving (drying) a particular portion of the porous media.

From Parlange and Hill (1976), Liu et al. (1994a), and Chandler et al. (1998) the scaling of finger width into the water and oil system is then given by,

$$\frac{d_{oil}}{d_{air}} = \frac{R\dfrac{\sigma_{w/o}}{\sigma_{w/a}}}{1 - \dfrac{\rho_o}{\rho_w} - \dfrac{v(\theta_{w_f} - \theta_{w_i})}{K(\theta_{w_f})}} \tag{4}$$

where v is the velocity of the finger, d_{oil} is the finger width for the water–oil system, and d_{air} is the finger width for the water–air system. $K(\theta_{w_f}) = k\rho g/\mu$ is the water conductivity behind the wetting front where k is the permeability. This expression has been derived in the low velocity limit, where the effect of viscosity of the displaced fluid on the water flow is assumed to be negligible.

We also wish to understand the fluid distribution within the preferential flow path. For water infiltrating an air-dry soil, Selker et al. (1992b) provided a description of the water content behind a moving gravity-driven finger. We follow their arguments for the case of water infiltrating an oil-saturated soil.

Starting with the one-dimensional Richards' equation,

$$\frac{\partial\theta_w}{\partial t} = \frac{\partial}{\partial z}\left(K(\theta_w)\frac{\partial\Phi_w}{\partial z}\right) \tag{5}$$

where z is the vertical distance (positive downward), $K(\theta_w)$ is the unsaturated conductivity for water, and Φ_w is the total (or hydraulic) potential in units of head in the water phase (cm water). To solve Eq. (5) Φ_w needs to be expressed in terms of capillary pressure, non-wetting phase potential and gravity potential. The total potentials for water and the non-wetting phase are given by

$$\Phi_w = -z + h_w \tag{6}$$

$$\Phi_o = -\frac{\rho_o}{\rho_w} z + h_o \tag{7}$$

and using the definition of capillary pressure in Eq. (2), we can put the total water potential in terms of the phase densities, the capillary pressure, and the non-wetting phase potential,

$$\Phi_w = -\left(1 - \frac{\rho_o}{\rho_w}\right) z - h_c + \Phi_o . \tag{8}$$

Substituting Eq. (8) into Eq. (5) gives

$$\frac{\partial \theta_w}{\partial t} = \frac{\partial}{\partial z}\left(-K(\theta_w)\left(1 - \frac{\rho_o}{\rho_w} + \frac{\partial h_c}{\partial z} - \frac{\partial \Phi_o}{\partial z}\right)\right) \tag{9}$$

We have observed that for fingered water flow into light oil the pressure in the oil is hydrostatic, thus, the last term $\partial\Phi_o/\partial z$ is zero in Eq. (9). Moreover, it has been experimentally observed that the fluid content profile within the finger translates downward at a constant velocity, v, and, thus, the water content and capillary pressure can be expressed as $\theta(\eta)$ and $h_c(\eta)$ with $\eta = z - vt$. Then, with this change in coordinate axes, the partial differential Eq. (9) is converted into an ordinary differential equation,

$$v\frac{d\theta_w}{d\eta} = \frac{d}{d\eta}\left(K(\theta_w)\left(1 - \frac{\rho_o}{\rho_w} + \frac{dh_c}{d\eta}\right)\right). \tag{10}$$

Integrating and rearranging yields,

$$v\theta_w = K(\theta_w)\left(1 - \frac{\rho_o}{\rho_w} + \frac{dh_c}{d\eta}\right) + C \tag{11}$$

where C is the constant of integration. The constant is evaluated for infiltration into oil saturated soil that at $\eta = \infty$, $\theta_w = 0$, and $dh_c/d\eta = 0$, which yield $C = 0$. Eq. (11) reduces to:

$$v\theta_w = K(\theta_w)\left(1 - \frac{\rho_o}{\rho_w} + \frac{dh_c}{d\eta}\right) \tag{12}$$

which relates the water content, the finger velocity, the unsaturated conductivity, and the capillary pressure within the finger. This expression can be used to calculate the extent of the finger tip and the unsaturated conductivity, among other things.

At a particular time, t, the capillary pressure within the finger path is given by,

$$\frac{\mathrm{d}h_c}{\mathrm{d}\eta} = -1 + \frac{\rho_o}{\rho_w} + \frac{\upsilon\theta_w}{K(\theta_w)}. \quad (13)$$

Since a column of water at rest has $\mathrm{d}h_c/\mathrm{d}z = -1 + \rho_o/\rho_w$, the above equation predicts that the water content within the finger will appear as a capillary rise ''stretched'' by the velocity term in Eq. (13). For soils, the lower portion of a water column (or, equivalently, the h_c–θ relationship) has a region of constant fluid content between the water entry pressure and the oil entry pressure. This region of constant water content, θ_f, has been observed in fingers in air-dry soil. Since the water content is constant, by integrating Eq. (13), we obtain a prediction for the length of the tip region for water fingers through oil-saturated sand,

$$L_{tip} = \frac{h_c(\text{o.e.}) - h_c(\text{w.e.})}{1 - \frac{\rho_o}{\rho_w} - \frac{\upsilon\theta_{w_f}}{K(\theta_{w_f})}} \quad (14)$$

where L_{tip} is the expected length of the finger tip, and h_c(w.e.) and h_c(o.e.) are the water-entry and oil-entry pressures, respectively. Assuming the capillary pressure–fluid content scaling in Eq. (3), L_{tip} can be calculated from the known water and air entry values in the water–air system, the densities, the finger velocity and fluid content, and the conductivity of the soil.

If the fluid pressures are also measured, it is possible to obtain measurements for the unsaturated conductivity using Eq. (12).

3. Materials and methods

Experiments to observe and measure finger properties were performed in two different two-dimensional chambers uniformly packed with sand. Both sample chambers had 0.94 cm thick polycarbonate walls, an interior thickness of 0.94 cm, and height of 55 cm, but different widths of 30 and 51 cm. Attached to the bottom end of each chamber was a manifold of five fluid ports, and the top end was left open to the atmosphere. Chambers were packed as follows: The bottom of the chamber was filled to a height of 17 cm with Soltrol 220 (Phillips), a non-toxic light NAPL. Clean, dry, sieved, quartz sand (Unimin) was dropped through the top using a dual randomizing funnel in a single pour to minimize layering. During packing and for 1 min afterwards, the chamber was vibrated to enhance settling. Grain sizes of 12/20 and 20/30 sand were used, where the numbers correspond to the sieve sizes the sand passes through and does not pass through, respectively. This produced a tight oil-saturated pack with minimal entrapped air and a porosity of 37%. Water fingers in these sand packs had uniform widths and velocities throughout the chamber.

The aqueous solutions used in the experiments consisted of either water or water with a dissolved surfactant. In all cases, a solution of 0.005% of FD&C blue #1 dye was

added to aid in the visual inspection of water positions. Four commonly available surfactants were used: Alfonic 810-4.5 Ethoxylate (CONDEA Vista) and Surfynol 485 (Air Products and Chemicals) are ionic surfactants, and Neodol (R) 25-7 (Shell Chemical) and Poly Sodium Vinyl Sulfonate (Air Products and Chemical) are non-ionic. The names have been abbreviated throughout the text as alfonic, surfynol, neodol, and sulfonate, respectively. The surfactants were mixed with water to a 1% by weight solution. Interfacial tensions between each solution and Soltrol 220 were measured using a ring (du Nouy ring method) tensiomat. To distinguish the fingers for different surfactants, we use the notation ''surfactant fingers'' (for example ''surfynol finger'') meaning the finger was formed when the infiltrating water contained 1% of the particular surfactant. ''Water fingers'' are generated when only water was added.

Infiltrations of the aqueous solution were performed by applying the aqueous solution to the top of the chamber either uniformly or through a point source. Uniform applications were performed in the wider chamber (width = 51 cm). The application system consisted of a peristaltic pump-driven point source, where a rotating camshaft moved continuously across the soil surface. Uniform application rates were 5.6, 9.4, and 13 cm/h for the water without surfactants and 2.25, 6.0, and 10.0 cm/h for water with surfactants. Oil was removed from the bottom of the chamber through a constant head overflow system at the height of the soil surface. For uniform applications, the chamber was placed in front of a light source and the infiltrations were visually observed.

Point source applications were performed in the smaller chamber (width = 30 cm). In this case, the water application system was set up to keep the fluid content in the chamber constant. This consisted of a fixed peristaltic pump which applied the solution through a tube and needle at 2 ml/min. The other end of the pump tubing was connected to the bottom of a stoppered 250 ml Erlenmeyer flask containing the aqueous solution, which was, in turn, connected to the bottom of the chamber, thus pulling an equal amount of oil out of the chamber. Using this system to withdraw oil from the bottom of the chamber, as water was being applied to the top, maintained a constant fluid level.

For the point source infiltrations, fluid contents were measured using synchrotron X-ray attenuation. The dual energy attenuations were obtained at the F-2 beam line of the Cornell High Energy Synchrotron Source using a set-up described in detail elsewhere (DiCarlo et al., 1997). The chamber was mounted on a movable platform which had a vertical and horizontal range of 50 and 25 cm, respectively, and a position repeatability of 0.01 cm. In this experiment, we used X-ray energies of 25 and 50 keV, allowing two independent measurements of the medium. As the system consisted of two fluids, only the 25 keV X-ray attenuation was used to obtain the water content. The 50 keV X-ray was used for measuring the density of the soil and, thus, to account for shifting sand particles. For two-fluid measurements, the water content is related to the attenuation through

$$\theta_w = -\frac{A - A_0}{(\nu_w - \nu_o)\, x} \tag{15}$$

where A is the measured attenuation, A_0 is the attenuation through the oil saturated soil, x is the thickness of the chamber, and ν_w and ν_o are the measured 25 keV attenuation

constants for the water and oil phases, respectively. During the infiltrations, moisture contents were determined near the tensiometers. At the beginning and end of each experiment, horizontal scans were made.

Fluid attenuation constants were obtained using a polycarbonate chamber with five sequential cells of 0.56 cm thickness (Lenhard et al., 1988). The attenuation was measured for the empty chamber and after each cell was filled with either fluid. The measured attenuations were linear with fluid thickness, and the attenuation constant was given by the slope.

Water and oil pressures were obtained using four miniature tensiometers (Selker et al., 1992a) placed as pairs in opposing positions on either site in a line 40 cm above the bottom of the chamber. The pairs were 2 cm left of the horizontal center and on the center (on the front of the chamber). Each tensiometer consisted of a hollow brass housing, with one end connected to the soil through a 0.8 cm diameter porous plate, and the other end connected to a pressure transducer through a rigid plastic tube and a three-way valve. The other port of each three-way valve was connected to a vertical reservoir of water. Prior to each experiment, the valve was opened to the reservoir and the transducers were calibrated using different water heights in the reservoir. Water tensiometers were filled with degassed water, and had a sintered glass porous plate (Ace Glass) with a maximum pore size of 70–100 μm. Oil tensiometers were filled with Soltrol 220 and had a sintered stainless steel porous plate (Mott Metallurgical) with a pore size of 20 μm. As water preferentially wetted, the glass plate and oil preferentially wetted the stainless steel plate, each tensiometer provided a connection to their particular fluid within the sand pack. The capillary pressure was obtained by subtracting the water pressure from the oil pressure.

Finger widths were found by analyzing tracings from the experiments and from horizontal attenuation scans through the finger. Tracings were done on 1 cm graph paper taped on the back of the chamber. While the finger was infiltrating, the finger was then traced at 1 min intervals. The width was then measured from the paper tracings every vertical 5 cm. Horizontal attenuation scans were performed after the finger had reached the bottom of the chamber, and widths of the fingers were determined by taking the boundaries at half of the core water content in the finger at that depth. Both procedures produced similar results and the reported widths are an average of the two procedures.

4. Results

4.1. Uniform water applications

Due to the difficulties in applying water uniformly at the synchrotron and lack of control of the finger positions, only qualitative results were obtained for the uniform applications. When the aqueous solution was applied uniformly to the top of the oil-saturated 12/20 sand pack, for every solution the water moved through the soil pack in preferential paths. The experiments were repeated for three infiltration rates ranging from 2.2 to 13 cm/h. The widths of the fingers and the pattern of the fingers varied for each surfactant used.

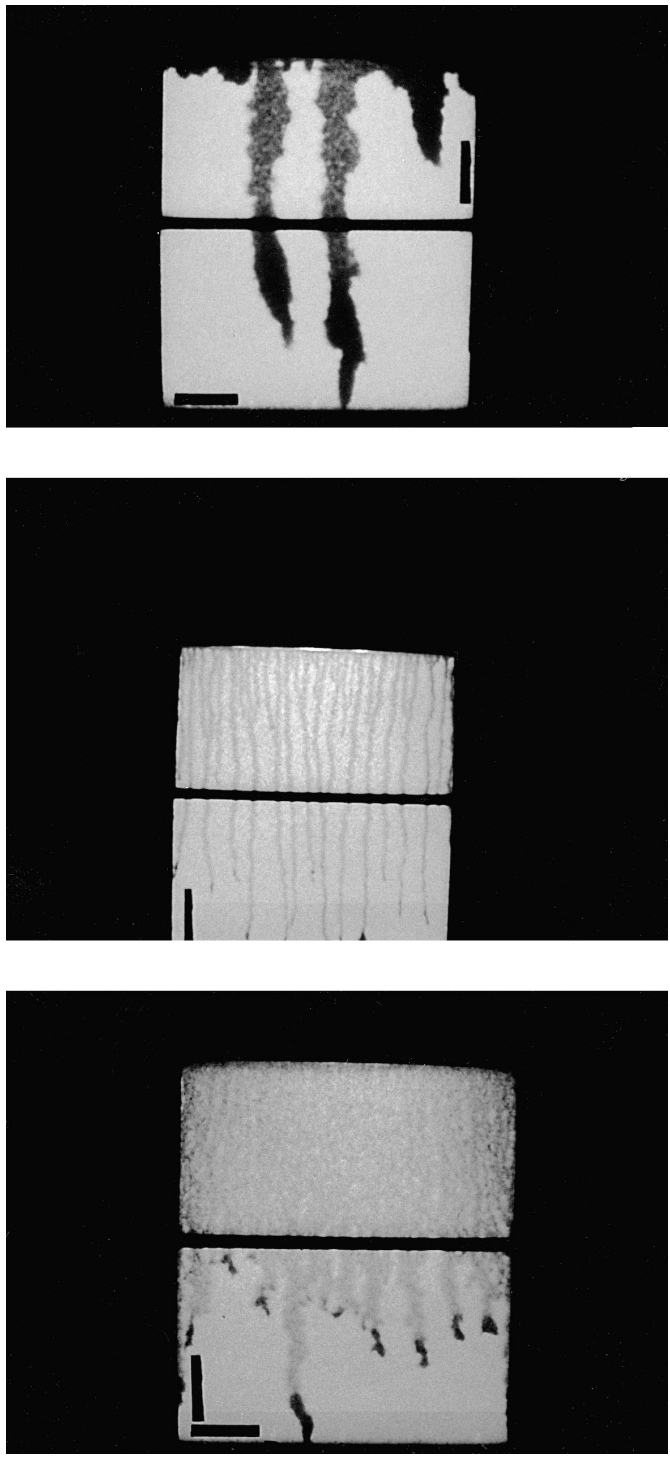

Table 1
Summary of the internal finger properties for each infiltrating fluid and for both sand sieve sizes

Fluid	Interfacial tension (dyn/cm)	Finger width (cm)	Finger tip length (cm)	Capillary pressure rise (cm H_2O)	Finger velocity (cm/s)
12 / 20 Sand					
Water	24	4.8	10.2	4.0	0.03
Sulfonate	21	2.8	8.0	2.6	0.055
Surfynol	9	2.4	8.0	1.5	0.06
Neodol	4	2.2	4.0	< 0.2	0.09
Alfonic	3	1.6	3.5	< 0.2	0.09
20 / 30 Sand					
Water	24	5.1	25	3.5	0.022
Sulfonate	21	4.2	28	3.5	0.025
Surfynol	9	5.0	13	1.8	0.03
Neodol	4	2.1	6	0.5	0.043
Alfonic	3	1.9	6	< 0.5	0.045

For pure water, the observed preferential flow moved through the chamber at a constant velocity and with constant widths between 5 and 8 cm. The flow paths are shown in Fig. 1a. No splitting or merging was observed. Higher infiltration rates just produced more fingers; infiltrations of 5.6, 9.4, and 13 cm/h produced one, two, and three fingers, respectively.

For the surfactant solutions, sulfonate produced only two fingers for an infiltration rate of 2.2 cm/h and five fingers (three of which moved downward) for an infiltration rate of 10 cm/h. Similar to the water solution, these fingers did not merge and kept the same width and velocity throughout the chamber. Initially, the surfynol solution produced 10 fingers for all flow rates with widths between 2 and 3 cm. Only a few fingers merged and 6 to 8 fingers remained at a depth of 50 cm with, roughly, the same width. The low interfacial tension solutions containing neodol and alfonic (Fig. 1b and c, respectively) were much different. Initially, each produced approximately 20 fingers having widths of 1 cm or less for all flow rates. Many of these fingers quickly merged and produced fewer and faster moving fingers. Typically, the finger merging occurred twice for each infiltration, a primary merge at a depth of 10 to 20 cm, and a secondary merge at a depth of 40 to 50 cm, most clearly visible for the alfonic as a surfactant (Fig. 1c).

4.2. Point source applications

All point source applications of the aqueous fluids produced preferential flow paths. Water, sulfonate, and surfynol each produced one single finger with uniform width and

Fig. 1. Sketch of fingering patterns when an aqueous solution is infiltrated uniformly on an oil-saturated sand: (a) water at 9.4 cm/h, (b) water with neodol as a surfactant at 6 cm/h, and (c) water with alfonic as a surfactant at 6 cm/h.

visually similar to the fingers observed for the uniform applications. Neodol and alfonic, however, exhibited different behavior from that observed in the uniform applications. Neodol began as one main finger, but small fingers quickly began to splinter off. These other fingers remained small and did not grow continuously during the experiment. Alfonic, similar to neodol, had many fingers which splintered off the main finger, but the fingers continued to grow and became the same size as the main finger, if not larger. The entire chamber became filled with alfonic fingers, and the entire finger pattern closely resembled a large net. The fingers were extremely diffuse and pervasive, especially when compared to the one water finger. Table 1 lists the widths and velocities of the main fingers. In general, water fingers were the widest followed by sulfonate, surfynol, neodol, and alfonic.

Water pressure and fluid content measurements were taken within the finger for each solution. Fig. 2 shows the water content and capillary pressure between the water and oil phases in the initial finger vs. time when the invading aqueous solution is distilled water (with the 0.005% blue dye). Both measurements were taken at $z = 40$ cm (40 cm above the bottom of the chamber). The behavior was qualitatively similar to that seen for water

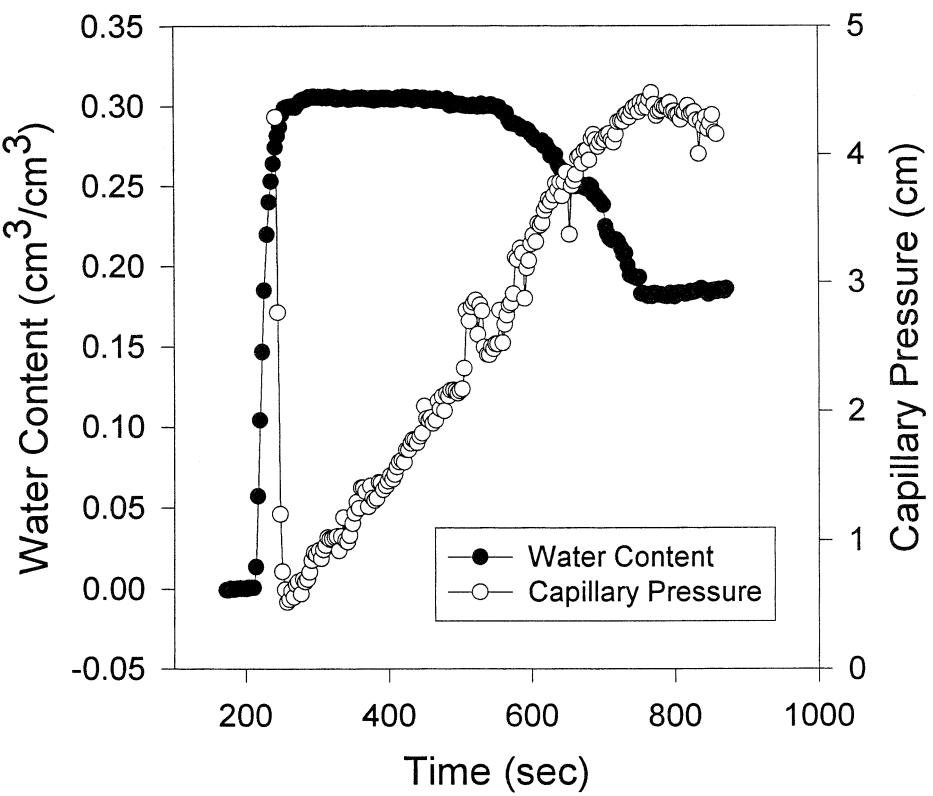

Fig. 2. Water content and capillary pressure inside a water finger infiltrating oil saturated 12/20 sand. The highest water content and capillary pressures are at the tip of the finger.

preferentially flowing through air-dry sand. The finger had a tip with a relatively constant water content of 0.30 cm^3/cm^3, behind which the water content quickly dropped to 0.17 cm^3/cm^3 where it leveled off. The capillary pressure was lowest at the finger tip (0.5 cm) and rose continuously after the tip before leveling off at 4 cm.

Fig. 3 shows the water content and capillary pressure within the finger when the invading aqueous solution contains 1% by weight surfynol. The same qualitative features, as seen in the water finger, are present: highly saturated tip, water content decreasing, and capillary pressure increasing behind the tip. The water content in the finger is quantitatively similar for the surfactant fingers with a tip water content of approximately 0.30 cm^3/cm^3 and water content directly behind the tip of 0.17 cm^3/cm^3. The surfactant fingers are quantitatively different from non-surfactant fingers in the actual length of the nearly saturated region at the tip, and the capillary pressure rise behind the tip.

Identical sets of water content and pressure data were taken for the other surfactant solutions and for a coarser sand pack of 12/20 sand. Table 1 lists the finger widths,

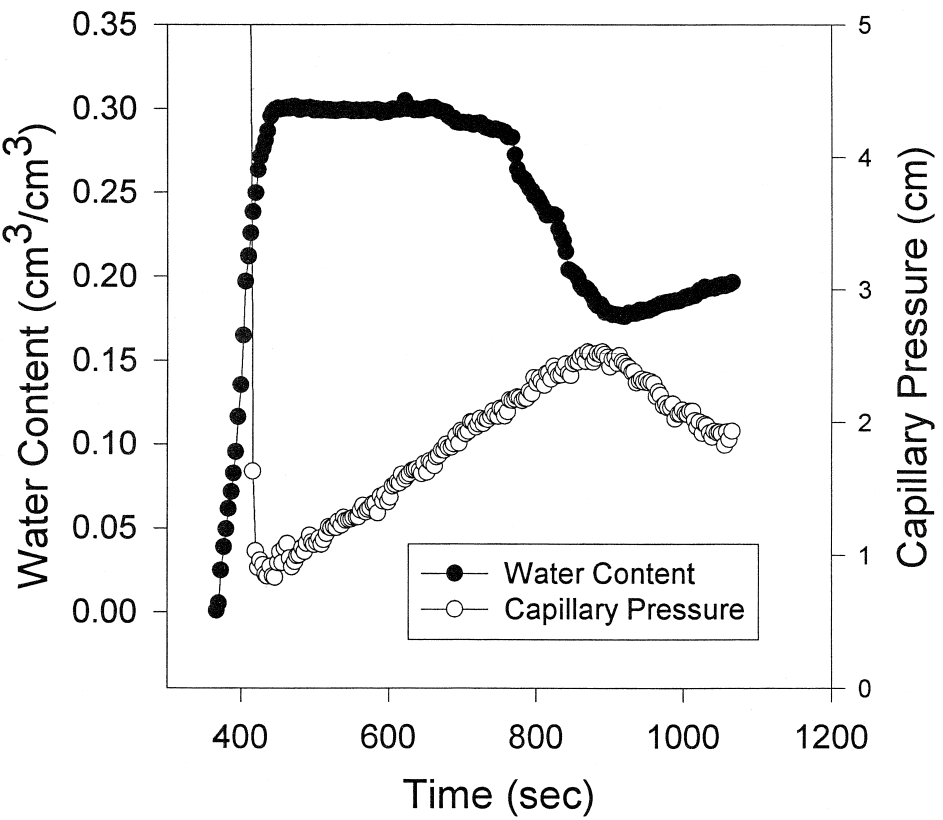

Fig. 3. Water content and capillary pressure inside a surfynol solution finger infiltrating oil saturated 12/20 sand. The pressure changes behind the tip are smaller than for the water case, and the water content of the surfynol solution rises slightly after the finger tip.

velocities, capillary pressure rises, and the lengths of the saturated tips for all of the data sets. The finger properties show definite trends with the interfacial tension of the fluids. As the interfacial tension between the solutions was lowered by the surfactants, the capillary pressure rose behind the wetting front, while the finger width and the length of the saturated tip decreased.

5. Discussion

Due to the qualitative similarity between the fingers observed here, and those observed in water infiltrating air-dry sand, we will analyze the data in the framework developed for the latter case. If this formulation is correct, the finger properties such as the finger width, the capillary pressure increase behind the finger, and the length of the finger tip should be scaled through the previous equations.

Fig. 4 shows the finger width vs. the interfacial tension for the 12/20 and 20/30 sand. The trend in the observed data follows the theoretical predictions; with the smallest fingers occurring with solutions of alfonic and neodol, which have the smallest interfacial tension values. At these low interfacial tensions is also where the predictions differ the most, with the fingers being wider than predicted. The lines are the predicted scaling relationship in Eq. (4). The widths of the water fingers through air-dry sand are, on the average, 1.8 and 2.3 cm for 12/20 and 20/30 sand, respectively (Rimmer et al., 1998). The interfacial tension and contact angles are somewhat uncertain as they change in time (Schroth et al., 1995). The lower lines in Fig. 4 are calculated with interfacial tensions in Table 1 and assume that the contact angles are the same (i.e., $R = 1$). The upper lines are obtained by matching soil characteristic curves of oil–water and air–water fluid pairs. Using the data in Schroth et al. (1996) and Rimmer et al. (1998), we find that R varies between 1.9 and 1.7 (we take $R = 1.8$). These R values include the effect of the unknown contact angles, however, they are only valid for the oil–water pair without any surfactants. Comparing the observed finger diameters, we find that they are generally higher than the values based on Eq. (4). We will discuss the possible reasons later.

The simultaneous measurements of capillary pressure and fluid content allow us to quickly obtain the capillary pressure–fluid content relationship for this water–oil system. Fig. 5 shows the measured relationship from the water infiltration and the re-infiltration into 12/20 sand. As the wetting process is very abrupt, both curves are on drying branches of the $h_c - \theta$ relationship.

Once the fingers are formed, hysteresis in the above capillary pressure–fluid content relationship is the reason that the finger does not expand once it is formed. In other words, the finger formed by an instability of the wetting front becomes quite stable in the consequent time. Here is why: The water does not enter the oil-saturated sand until the capillary pressure decreases to 0.5 cm, at which time the water enters at a water content of 0.30 cm^3/cm^3 (point A). Behind the finger tip, the capillary pressure increases and the water content decreases (point B). Since the capillary pressure behind the finger tip quickly becomes much greater than the water entry capillary pressure, the water is confined within the finger and cannot spread. The finger remains at point B

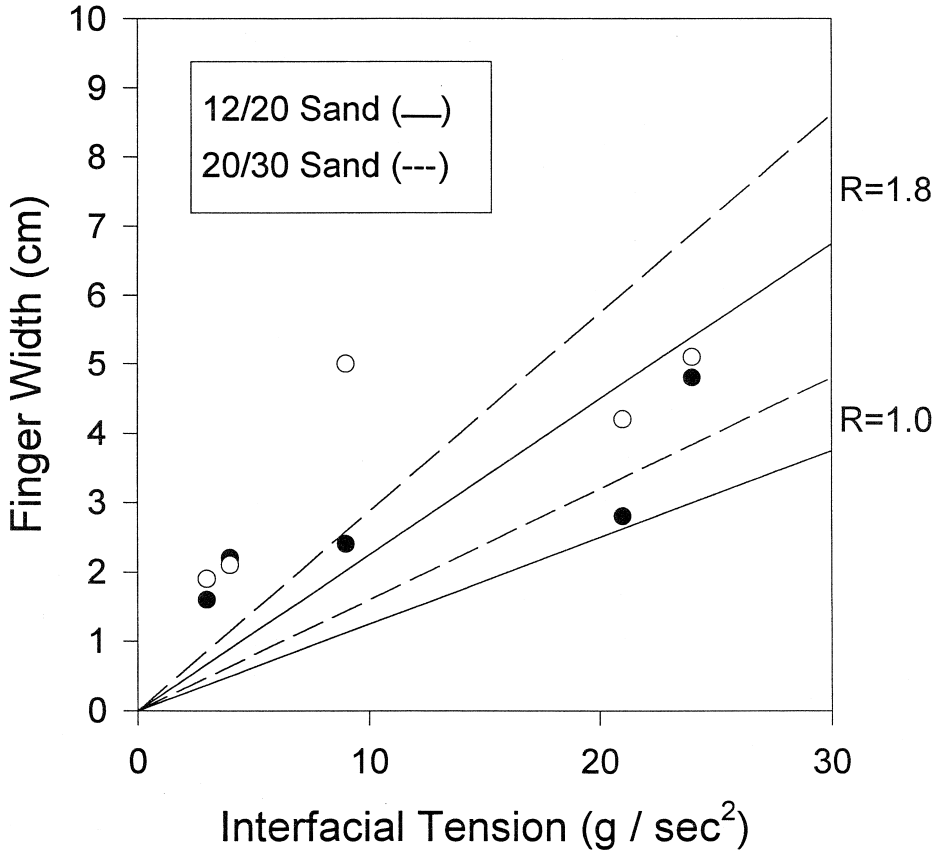

Fig. 4. Finger widths vs. interfacial tension for the five solutions and two sands used. The solid and dotted lines are the expected scaling from fingers in air-dry 12/20 (●) and 20/30 (○) sand, respectively. For the bottom two lines, $R = 1$; and for the two top lines, $R = 1.8$.

until the water is turned off, after which the capillary pressure increases and water content decreases further (point C). On a re-infiltration, the old finger core wets quickly to point D, where it remains until the water is turned off, after which it dries to point E. Again, on re-infiltration, the capillary pressure remains greater than the water entry capillary pressure and the water finger does not expand.

These capillary pressure increases differ for each surfactant used. Fig. 6 shows the maximum pressure rise inside the finger (Point A to Point B) vs. the interfacial tension of the fluids. The lines shown are the predicted dependence on interfacial tension obtained by scaling with Eq. (3) using as reference air–water fluid pair ($R = 1$) with a maximum drop of 9 cm for the 20/30 sand (Liu et al., 1994a) and 6 cm for the 12/20 sand (Chandler et al., 1998). As before, for the bottom lines, $R = 1$, and for the top lines, $R = 1.8$. The observed data on maximum pressure increase in the finger (Fig. 6) fits the scaling relationship well using as reference the observed pressure increase in an air–water system.

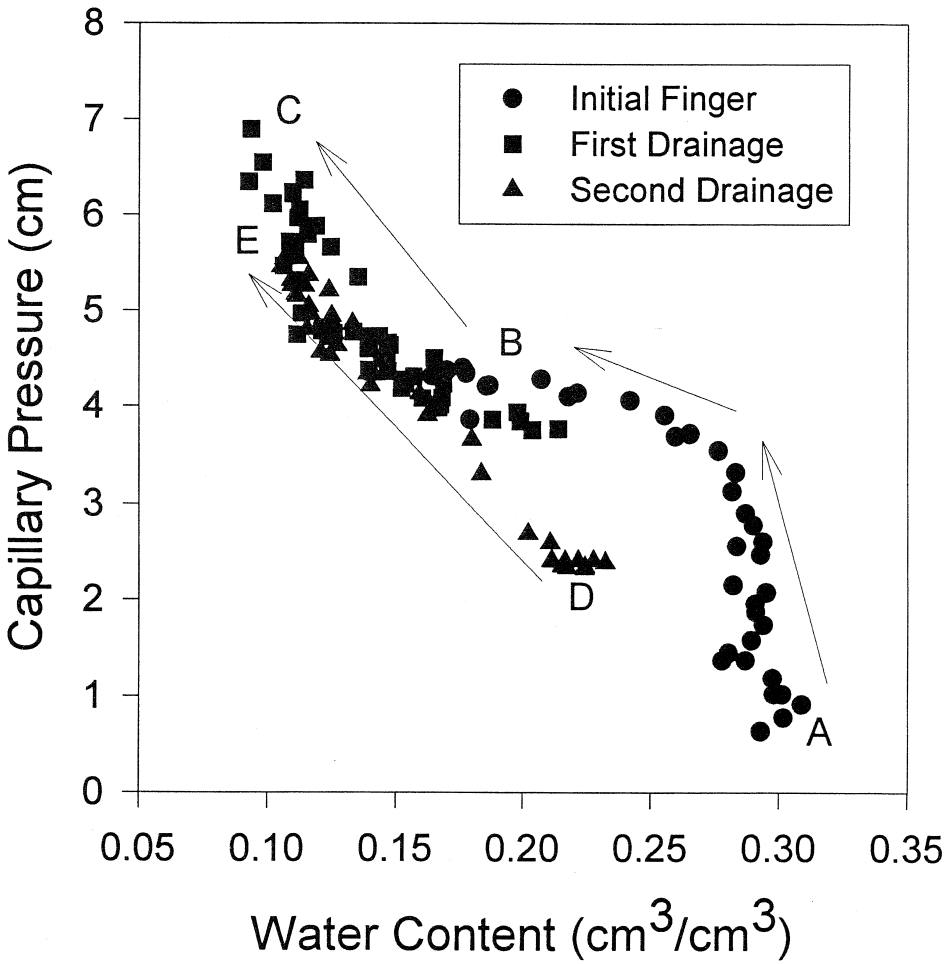

Fig. 5. Capillary pressure–fluid content relationship obtained from the water finger into oil-saturated 12/20 sand. The drying from A to B takes place in the initial finger, drying to point C occurs when the infiltration is stopped. Point D is reached on re-infiltration, and point E after the re-infiltration is stopped.

The capillary pressure data can give us insight into the finger patterns for different fluid pairs. For viscous fingering, it has been known for some time that at low interfacial tensions, the finger pattern becomes very unstable or ''chaotic'' with large amounts of finger splitting (Bensimon et al., 1986). For gravity-driven fingers, we also observed finger splitting at the lowest interfacial tensions. This splitting can be understood in terms of the water entry pressure of the soil and the capillary pressure rise inside the finger tips. For large interfacial tensions, the capillary pressure rise within the finger is large, and the capillary pressure behind the tip of the finger becomes greater than the water entry pressure. Therefore, there will not be enough pressure for the finger to expand, and the width will not increase. This is what is observed for infiltrations of

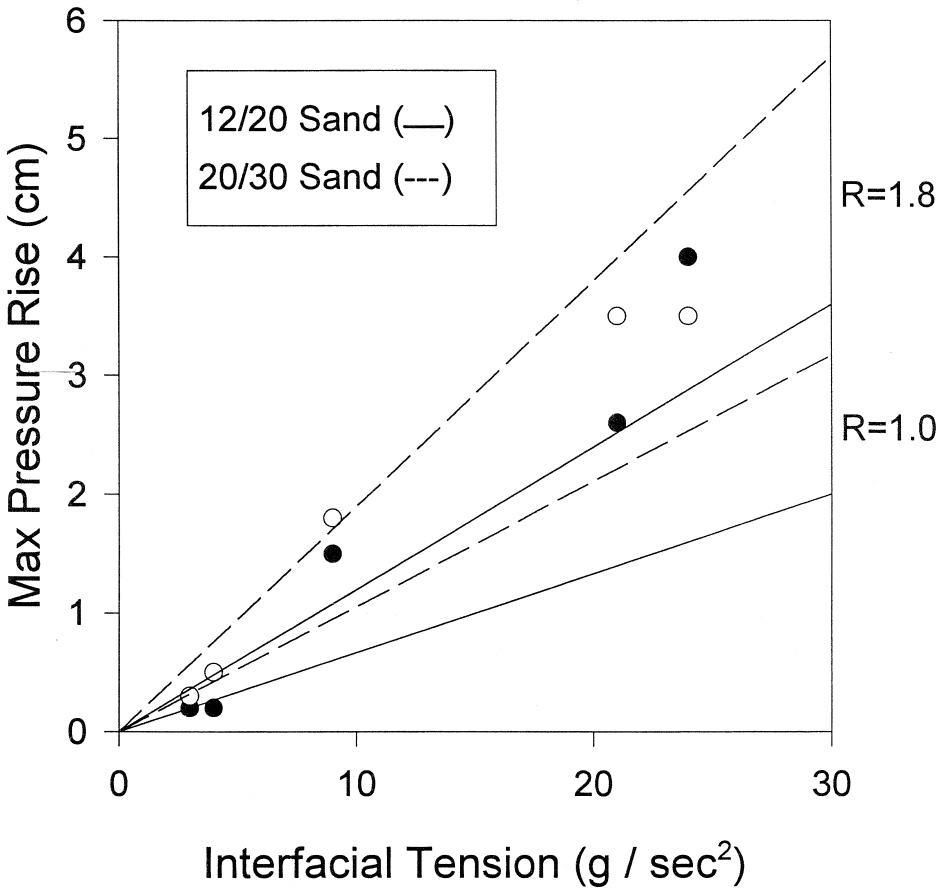

Fig. 6. Capillary pressure rises behind the finger tip vs. interfacial tension for the five solutions and two sands used. The solid and dotted lines are the expected scaling from fingers in air-dry 12/20 and 20/30 sand, respectively. For the bottom two lines, $R = 1$; and for the two top lines, $R = 1.8$.

surfynol, sulfonate, and water. For small interfacial tensions (e.g., neodol and alfonic), however, the capillary pressure rise within the finger is small, and the capillary pressure behind the tip of the finger remains close to or at the water entry pressure. Therefore, there will be enough pressure for the finger to expand, and splitting and secondary fingers can occur if the flow is slightly retarded by some inhomogeneity.

What is the role of viscosity in these gravity-driven fingers? In measurements of the oil pressure directly outside the finger path, we observed no change in the oil pressure as the finger passed (Chandler et al., 1998). Thus, for Soltrol and water with a viscosity ratio of $\mu_o/\mu_w = 4$, the major pressure changes are in the water phase and the assumption that the oil acts inviscidly (oil movement with little or no pressure gradients) during preferential flow, appears to be valid. Although there are no observed effects of oil viscosity in the bulk oil phase, other effects can be attributed to oil viscosity. The

most prominent of these viscous effects is that the finger is not completely saturated with water, unlike fingers in the water–air system. This is most likely due to the oil not being able to move out of the large pores fast enough during the infiltration because of its viscosity and snap-off.

The phenomenon is similar to air entrapment in an air–water system. The lower water content in the tip also affects the behavior of the finger behind the tip, as the lower tip water content yields a water conductivity of roughly half of the saturated conductivity.

Behind the finger tip, the water content drops and oil re-enters the finger path. Fig. 7 plots the measured length of the finger tip vs. that predicted in Eq. (12). Eq. (12) requires the difference between oil and water entry capillary pressures which can be

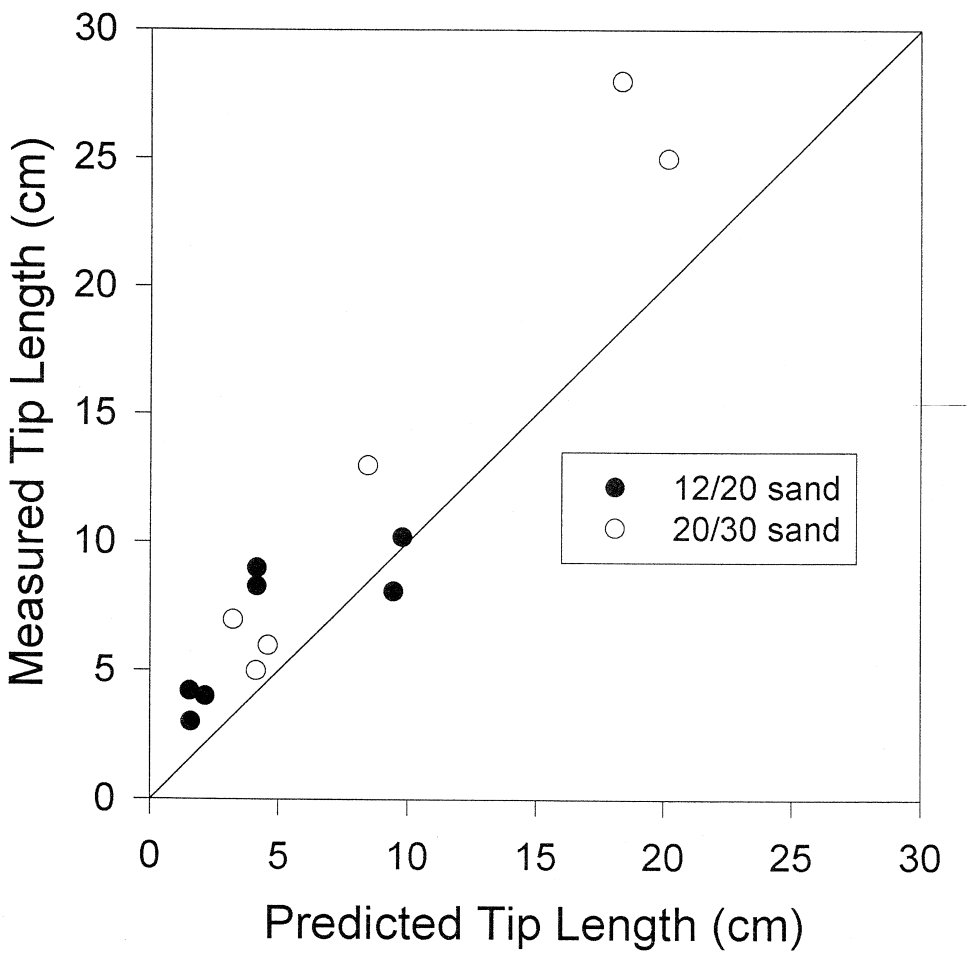

Fig. 7. Measured finger tip length vs. the predicted tip length from Eq. (8). Most tip lengths are slightly higher than predicted by the 1:1 solid line.

found by considering the capillary pressure and moisture content data in Figs. 2 and 3. The oil entry pressure occurs when the moisture content behind the finger tip starts to decrease from saturation. Figs. 2 and 3 show that this occurs when the capillary pressure is 70% of the maximum capillary pressure drop behind the finger. Thus, the difference in oil and water entry capillary pressures were obtained from multiplying the capillary pressure drop in Table 1 by 0.7. For the other parameter values in Eq. (12), we took a water content of 0.30 cm^3/cm^3, and the conductivity at this water content to be 0.45 and 0.15 cm/s for 12/20 and 20/30 sand, respectively. These were measured independently. Although in Fig. 7, the predicted data trend was similar to what was observed, the tip measured lengths were generally longer than the predicted lengths, except for the water and sulfonate in the 12/20 sand. The higher than predicted tip lengths is what would be expected if the displaced fluid has an appreciable viscosity or limited area for flow. Both will limit the rate at which oil can return into the finger path, thus making the finger longer. Especially, in the low interfacial tensions, many fingers formed (Fig. 1), decreasing the cross-sectional area for oil flow. The sulfonate and water fingers in the 12/20 sand were distinct and the oil had a large cross-sectional area to flow through in a medium with a high conductivity. Similar arguments based on viscosity and cross-sectional area can be made about why the finger diameter in Fig. 4 is larger than the theoretical width. As stated above, Eq. (4) is based on the assumption that there is no resistance to the movement of oil. When there is resistance to water by the oil, the finger will become wider (conceptually, this can be understood when the finger is a low conductivity medium — similar to a high viscosity — the finger will be equal to the width of the chamber). Especially, for the low interfacial tension where the resistance to oil movement is the highest (Fig. 1), we see, relatively, the largest discrepancies in finger width between the observed and theoretical values. Viscosity of the oil should have no effect on the maximum capillary pressure drop in the finger in Fig. 6. Indeed, we find that the values for the 20/30 sand are between the two theoretical extremes. The 12/20 sand is also close to the theoretical values.

In summary, when water is gravitationally driven through an oil saturated sand pack, fingers occur which resemble those seen when water infiltrates a dry sand pack. As opposed to viscous fingers in Hele–Shaw cells, behind the fingers tips oil re-enters the finger paths and the capillary pressure–fluid content relationship controls the spread of the fingers. These phenomena are well described by the theory developed for fingers from water infiltration with important scaling by the density differences, and the interfacial tensions, with the viscosity of the oil playing a minor role.

Acknowledgements

We would like to thank Edward Zhang, Qun Shen, and the staff at CHESS for useful discussions and experimental assistance. This work was supported (in part) by the Air Force Office of Scientific Research, USAF, under grant/contract number F49620-94-1-0291. CHESS is supported by NSF grant number DMR-931-1772. The careful reading and detailed comments of the reviewers is greatly appreciated.

References

Bauters, T.W.J., DiCarlo, D.A., Steenhuis, T.S., Parlange, J.-Y., 1999. Soil water dependent wetting front characteristics in sands. J. Hydrol., in press.

Bensimon, D., Kadanoff, L.P., Liang, S., Shraiman, B.I., Tang, C., 1986. Viscous flows in two dimensions. Rev. Mod. Phys. 58, 977–999.

Chandler, D.G., Cohen, Z., Wong, E., DiCarlo, D.A., Steenhuis, T.S., Parlange, J.-Y., 1998. Unstable fingered flow of water into a light oil. In: Morel-Seytoux, H. (Ed.), Eighteenth Annual American Geophysical Union Hydrology Days. Hydrology Days Publications, Atherton, CA, pp. 13–31.

Chuoke, R.L., van Meurs, P., van der Poel, C., 1959. The instability of slow, immiscible, viscous liquid–liquid displacements in permeable media. Trans. AIME 216, 188–194.

DiCarlo, D.A., Bauters, T.W.J., Steenhuis, T.S., Parlange, J.-Y., Bierck, B.R., 1997. High-speed measurements of three-phase flow using synchrotron x-rays. Water Resour. Res. 33, 569–576.

Glass, R.J., Steenhuis, T.S., Parlange, J.-Y., 1988. Wetting front instability as a rapid and far-reaching hydrologic process in the vadose zone. In: Germann, P.F. (Ed.), Rapid and Far-Reaching Hydrologic Processes in the Vadose Zone. J. Contam. Hydrol. 3, 207–226.

Hill, D.E., Parlange, J.-Y., 1972. Wetting front instability in layered soils. Soil Sci. Soc. Am. J. 36, 697–702.

Homsy, G.M., 1987. Viscous fingering in porous media. Annu. Rev. Fluid Mech. 19, 271–311.

Lenhard, R.J., Parker, J.C., 1987. A model for hysteretic constitutive relations governing multiphase flow: 2. Permeability–saturation relations. Water Resour. Res. 23, 2197–2206.

Lenhard, R.J., Dane, J.H., Parker, J.C., Kaluarachchi, J.J., 1988. Measurement and simulation of one-dimensional transient three-phase flow for monotonic drainage paths. Water Resour. Res. 24, 853–863.

Liu, Y., Steenhuis, T.S., Parlange, J.-Y., 1994a. Closed form solution for finger width in sandy soils at different water contents. Water Resour. Res. 30, 949–952.

Liu, Y., Steenhuis, T.S., Parlange, J.-Y., 1994b. Formation and persistence of fingered flow fields in coarse grained soils under different moisture contents. J. Hydrol. 159, 187–195.

Parlange, J.-Y., Hill, D.E., 1976. Theoretical analysis of wetting front instability in soils. Soil Sci. 122, 236–239.

Rimmer, A., DiCarlo, D.A., Steenhuis, T.S., Bierck, B., Durnford, D., Parlange, J.-Y., 1998. Rapid fluid content measurement method for fingered flow in an oil–water–sand system using synchrotron x-rays. J. Contam. Hydrol. 31, 315–335.

Saffman, P.G., Taylor, G.I., 1958. The penetration of a fluid into a porous medium or Hele–Shaw cell containing a more viscous liquid. Proc. R. Soc. London, Ser. A 245, 312–329.

Schroth, M.H., Istok, J.D., Ahearn, S.J., Selker, J.S., 1995. Geometry and position of light nonaqueous-phase liquid lenses in water-wetted porous media. J. Contam. Hydrol. 19, 269–287.

Schroth, M.H., Ahearn, S.J., Selker, J.S., Istok, J.D., 1996. Characterization of Miller-similar silica sands for laboratory hydrologic studies. Soil Sci. Soc. Am. J. 60, 1331–1339.

Selker, J.S., Leclerq, P., Parlange, J.-Y., Steenhuis, T.S., 1992a. Fingered flow in two dimensions: Part 1. Measurements of matric potential. Water Resour. Res. 28, 2513–2521.

Selker, J.S., Parlange, J.-Y., Steenhuis, T.S., 1992b. Fingered flow in two dimensions: Part 2. Predicting finger moisture profile. Water Resour. Res. 28, 2523–2528.

Stokes, J.P., Weitz, D.A., Gollub, J.P., Dougherty, A., Robbins, M.O., Chaikin, P.M., Lindsay, H.M., 1986. Interfacial stability of immiscible displacement in a porous media. Phys. Rev. Lett. 57, 1718–1721.